tively. The partial molal enthalpies of water in methanol, ethanol, and propanol-2 at infinite dilution of water increase with the molecular weight of the alcohol and are −680, −400, and +400 cal. per mole, respectively.

The asymmetry of the curves on a ΔH^M *vs.* x_1 plot (Figure 4) increases with the increase of molecular weight of the alcohols. Interpolated ΔH^M values for propanol-1-water (*2*) are also included in Figure 4 for comparison. For aqueous solutions of nonelectrolytes, Rowlinson (*7, 12*) suggested that the increase of the proportion of CH_2 groups in the molecules makes hydrogen bonding more difficult for steric reasons. If the solute (alcohol) is capable of forming a small number of reasonably strong hydrogen bonds to water, ΔH^M is generally positive in mixtures rich in solute and negative in mixtures rich in water. Propanol-1 and water and propanol-2 and water systems follow this behavior. An increase in the strength or number of the solute-water bonds leads to negative ΔH^M values over the complete concentration range. Methanol-water and ethanol-water systems follow this behavior.

Excess Free Energy of Mixing, ΔG^E. Vapor-liquid equilibrium data reported at 25° C. by Butler, Thomson, and MacLennan (*4*) for the system methanol-water and by Dobson (*6*) for the system ethanol-water were smoothed and used for obtaining the ΔG^E values. For the system propanol-2-water, vapor-liquid equilibrium data reported by Wilson and Simmons (*13*) at 95 and 190 mm. of Hg were used together with the heat of mixing data of this investigation for obtaining the ΔG^E values at 25° C. This method of calculation has been reported previously (*9*). The values obtained for these systems are graphically presented in Figure 5. ΔG^E values for propanol-1-water are also included in Figure 5. They were evaluated from the vapor-liquid equilibrium data reported by Butler and coworkers (*4*). The ΔG^E values increase with the increase of the molecular weight of the alcohols, and all ΔG^E values are positive. The ΔG^E values for propanol-2-water are between that for ethanol-water and propanol-1-water.

Excess Entropies of Mixing, ΔS^E. Excess entropies of mixing are evaluated from the relationship

$$T\Delta S^E = \Delta H^E - \Delta G^E$$

and are graphically presented in Figure 6. All the values are negative. A decrease in the strength of alcohol-water bonds leads to an increasing of the excess entropy, with the exception of methanol.

ACKNOWLEDGMENT

The authors wish to thank the National Research Council of Canada for financial support.

LITERATURE CITED

(1) Benjamin, L., Benson, G.C., *J. Phys. Chem.* **67**, 858 (1963).
(2) Bose, E., *Z. Physik. Chem.* **58**, 585 (1907).
(3) Bosjnakovic, F., Grumbt, J.A., *Forsch. Gebiete Ingenieurw.* **2**, 421 (1931).
(4) Butler, J.A.V., Thomson, D.W. Maclennan, W.H., *J. Chem. Soc. (London)* **1933**, p. 674.
(5) Dimmling, Werner, Lange, E., *Z. Elektrochem.* **55**, 322 (1951).
(6) Dobson, H.J.E., *J. Chem. Soc.* **127**, 2866 (1925).
(7) Hadzi, D., Ed., "Hydrogen Bonding," p. 423, Pergamon Press, London, 1959.
(8) Katayama, T., *Chem. Eng. Japan* **26**, 361 (1962).
(9) Lu, B.C.-Y., *Can. J. Chem. Eng.* **37**, 193 (1959).
(10) McDonald, J.E., King, J.F., Cobble, J.W., *J. Phys. Chem.* **64**, 1345 (1960).
(11) Ocon, J., Taboada, C., *Anales Real Soc. Espan. Fis. Quin. (Madrid)* **55B**, 108, 243 (1955).
(12) Rowlinson, J.S., "Liquids and Liquid Mixtures," pp. 183–6, Butterworths, London, 1959.
(13) Wilson, A., Simons, E.L., *Ind. Eng. Chem.* **44**, 2214 (1952).

RECEIVED for review November 10, 1964. Accepted March 22, 1965.

The Condensed System LiF–NaF–ZrF_4—Phase Equilibria and Crystallographic Data

R. E. THOMA, H. INSLEY, H. A. FRIEDMAN, and G. M. HEBERT

Reactor Chemistry Division, Oak Ridge National Laboratory, Oak Ridge, Tenn.

THE potentialities of the system LiF-NaF-ZrF_4 in molten-salt technology have been recognized and developed during the last several years. As molten solvents for ZrF_4, LiF and NaF are cheap, stable, and in combination provide a high capacity for ZrF_4. Initially of interest as a nuclear reactor fuel solvent (*9*), the system LiF-NaF-ZrF_4 has recently been adapted with marked success in chemical reprocessing of spent reactor fuel elements (*6, 14*). Although no previous comprehensive report has been made of the phase equilibria in the system LiF-NaF-ZrF_4 and the limiting binary system LiF-ZrF_4, several interim reports have indicated the progress of this investigation (*8, 19*). Precise definition of the equilibrium relationships in the ternary system has required a long and tedious investigation, because of the formation of complex solid solutions on the one hand and the difficulty of obtaining very pure reagents on the other.

This report presents composition-temperature diagrams of the system LiF-NaF-ZrF_4 and the limiting binary system LiF-ZrF_4. Phase behavior in these systems was investigated in the temperature range from the liquidus down to about 400° C. This lower temperature limit was chosen because, at temperatures below this, solid-state equilibria in these systems are established only during impractically long annealing periods.

Nine complex fluoride compounds have been observed to crystallize from molten mixtures of LiF, NaF, and ZrF_4. Unquestionably, reasons for the complex phase behavior among crystalline solids in the LiF-NaF-ZrF_4 system will be obtainable only through studies of the crystal chemistry of these nine fluorides. The structures of only two of these crystalline phases, $3NaF \cdot ZrF_4$ (*10*) and $2LiF \cdot ZrF_4$ (*12*), have been elucidated. Single-crystal studies of the compound $7NaF \cdot 6ZrF_4$ have been in progress for some

Equilibrium phase diagrams of the ternary system LiF–NaF–ZrF_4 and the limiting binary system LiF–ZrF_4 are presented. Equilibria among the condensed phases in the systems were established through the temperature interval from the liquidus to approximately 400° C. Composition-temperature relationships were established for the 4 invariant reactions of the LiF–ZrF_4 system and the 9 invariant reactions of the LiF–NaF–ZrF_4 system. Three equilibrium compounds were observed to form from LiF and ZrF_4—namely, $3LiF \cdot ZrF_4$, $2LiF \cdot ZrF_4$, and $3LiF \cdot 4ZrF_4$. A single ternary compound, $LiF \cdot NaF \cdot 4ZrF_4$, was isolated from crystallized salt mixtures. Complex solid solutions are formed between LiF–ZrF_4 and NaF–ZrF_4 compounds. Solution behavior is attributed principally to substitutional mechanisms. Representative optical and x-ray diffraction data are presented for all solid phases encountered in the ternary system.

time, but nothing is known of the remaining group of materials. Further investigations in the LiF–NaF–ZrF_4 system should therefore begin with the crystal chemistry of the system.

EXPERIMENTAL

Materials. The alkali fluorides used in these investigations were of reagent grade obtained from several commercial vendors. In all cases, spectrographic and chemical analyses were obtained which indicated that the component reagents were essentially free of contaminant cations (<500 p.p.m. total). Pure zirconium tetrafluoride was prepared by sublimation at low pressure in nickel equipment of the crude ZrF_4 obtained by treatment at 400° C. of commercial $ZrCl_4$ with anhydrous HF vapor. No impurities in the sublimed product were observed by x-ray diffraction and microscopic analysis (using the polarizing light microscope). Because zirconium fluoride is easily hydrolyzed to oxyfluorides or oxide at elevated temperatures, it was necessary to remove small amounts of water as completely as possible from starting materials. To convert small amounts of oxide or oxyfluoride to the fluoride, ammonium bifluoride was added to mixtures of LiF–ZrF_4 and LiF–NaF–ZrF_4 before initial heating in the thermal analysis experiments. The oxides were converted by the reaction with ammonium bifluoride to products which have not been identified but which are presumably ammonium fluorometallates. Upon further heating, the ammonium fluorometallates decomposed to form metal fluorides. To prevent the re-formation of oxides or oxyfluorides after the ammonium bifluoride was removed, the mixtures were melted and cooled under a dry helium atmosphere. The purified mixtures for which thermal analysis data had been obtained were used subsequently in preparation of specimens for the quenching experiments. The handling procedure was controlled so that a frozen melt was exposed to laboratory air after removal of the ammonium bifluoride only during the 15- to 20-minute period required to transfer the ingot in its graphite crucible at approximately 400° C. from the furance to a helium-filled dry box; here, homogeneous powders were prepared for use in annealing-quenching experiments by grinding the entire ingot to <100 mesh. Water content of the dry box atmosphere was monitored continuously by a commercial moisture analyzer which employs an electrolytic cell. Manipulations in the dry box were performed only after

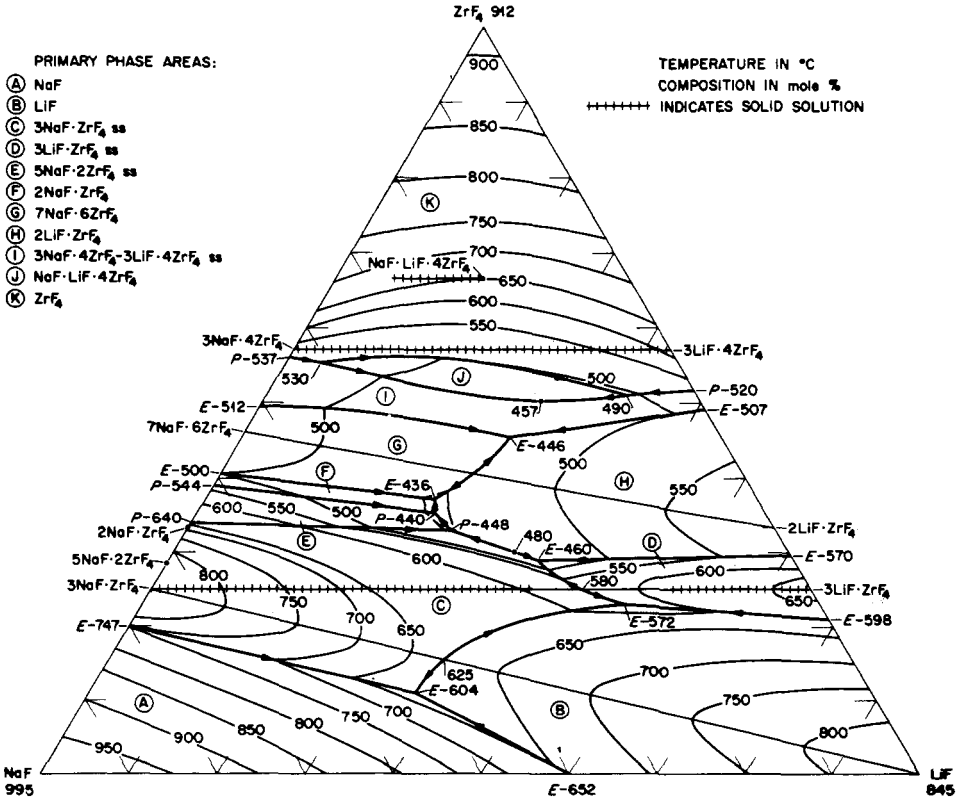

Figure 1. The system LiF–NaF–ZrF_4

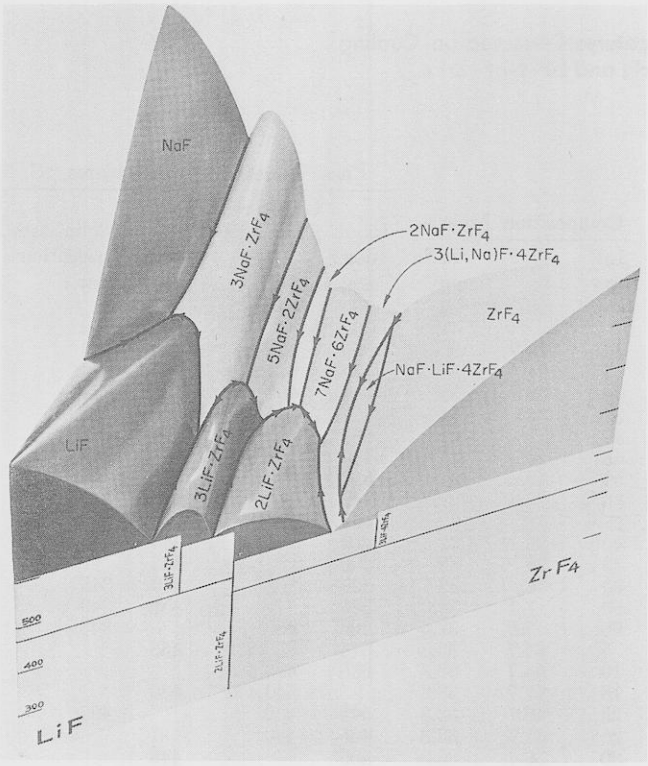

Figure 2. Three-dimensional model of the system LiF–NaF–ZrF_4

moisture concentration in the blanket atmosphere was reduced to <100 p.p.m.

APPARATUS AND METHODS

The techniques used for measurement of the temperatures which define the LiF–ZrF_4 and LiF–NaF–ZrF_4 phase diagrams, as well as the x-ray and microscopic techniques used in identifying phases, have been discussed previously (*2, 7, 13*). Chromel-alumel thermocouples were used throughout the study, a period of several years. Manufacturers estimate the accuracy of stock chromel-alumel thermocouples to be within 0.5% in the temperature range 400 to 800° C. The accuracy and precision of the thermocouples used were routinely checked by calibration with well-known standards, NaCl and KCl. Typical statistical data from the averages of 10 melting point determinations with each of these reagents indicated melting points of 771° ± 2° and 801° ± 3° C., respectively, as compared with standard values for their melting points of 770.3° and 800.4° C. Reversibility of phase reaction equilibria involving LiF–NaF–ZrF_4 solid phases was demonstrated by the reproducibility of phase transition temperatures as determined in thermal analysis and in thermal-gradient-quenching experiments. In the former, liquid-solid transitions were manifest by thermal arrests in the cooling curve for specimens which had been homogeneous liquids. With the latter method, these same transition temperatures were reproduced in specimens elevated to the same temperature intervals, annealed, and quenched.

DISCUSSION OF RESULTS

General. A polythermal projection of the LiF–NaF–ZrF_4 phase diagram showing the liquidus surface is given in Figure 1, and a three-dimensional model of the system is shown in Figure 2. Compositions and temperatures of LiF–ZrF_4 and LiF–NaF–ZrF_4 invariant and singular points are listed in Table I. These phase diagrams were constructed on the basis of phase transition data obtained from thermal analysis and thermal-gradient-quenching experiments (Tables II and III). Figures 1 and 2 show that reactions at the liquidus surface of the LiF–NaF–ZrF_4 system are largely those associated with the limiting binary systems. The phase diagram of the system NaF–LiF (*4*) is characterized by a single invariant point, the eutectic at 652° C. and 60 mole % LiF. The phase diagram of the limiting system NaF–ZrF_4, reported previously from this Laboratory (*3*), is shown in Figure 3, and the phase diagram of the limiting system LiF–ZrF_4, not heretofore reported, is shown in Figure 4.

Crystallization equilibria in the system LiF–NaF–ZrF_4 are rather complex as a result of the number and variety of crystal phases of varying composition which may precipitate from these molten fluorides. The relative ease with which

Table I. Invariant and Singular Points in the Systems LiF–ZrF_4 and LiF–NaF–ZrF_4

Composition, Mole %					
LiF	NaF	ZrF_4	Temp., ° C.	Type of Equilibrium	Solids Present at Invariant Temperatures
79		21	598	Eutectic	LiF, α-3LiF·ZrF_4
75		25	662	Congruent melting point	α-3LiF·ZrF_4
			475	Inversion	α-3LiF·ZrF_4, β-3LiF·ZrF_4
			470	Decomposition	β-3LiF·ZrF_4, LiF, 2LiF·ZrF_4
70.5		29.5	570	Eutectic	α-3LiF·ZrF_4, 2LiF·ZrF_4
66.7		33.3	596	Congruent melting point	2LiF·ZrF_4
51		49	507	Eutectic	2LiF·ZrF_4, 3LiF·4ZrF_4
48.5		51.5	520	Peritectic	ZrF_4, 3LiF·4ZrF_4
			466	Decomposition	β-3LiF·4ZrF_4, 2LiF·ZrF_4, ZrF_4
37	52	11	604	Eutectic	NaF, LiF, 3NaF·ZrF_4
38	46.5	15.5	625	Boundary curve maximum	LiF, 3NaF·ZrF_4
55	22	23	572	Eutectic	α-3LiF·ZrF_4, 3NaF·ZrF_4 ss, LiF
49	26	25	580	Boundary curve maximum	α-3LiF·ZrF_4 ss, 3NaF·ZrF_4 ss
42	29	29	460	Eutectic	β-3LiF·ZrF_4 ss, 3NaF·ZrF_4 ss, 2LiF·ZrF_4
38.5	31.5	30	480	Boundary curve maximum	3NaF·ZrF_4 ss, 2LiF·ZrF_4
30	37	33	448	Peritectic	3NaF·ZrF_4ss, α-5NaF·2ZrF_4 ss, 2LiF·ZrF_4
27	37.5	35.5	440	Peritectic	2NaF·ZrF_4, α-5NaF·2ZrF_4 ss, 2LiF·ZrF_4
26	37	37	436	Eutectic	2NaF·ZrF_4, 7NaF·6ZrF_4, 2LiF·ZrF_4
29	30.5	40.5	470	Boundary curve maximum	7NaF·6ZrF_4, 2LiF·ZrF_4
30.5	24	45.5	446	Eutectic	7NaF·6ZrF_4, 3(Na, Li)F·4ZrF_4 ss, 2LiF·ZrF_4
32	18	50	457	Boundary curve minimum	LiF·NaF·4ZrF_4 ss, 3(Li, Na)F·4ZrF_4 ss
41	8	51	490	Peritectic	3(Li, Na)F·4ZrF_4 ss, LiF·NaF·4ZrF_4, ZrF_4
4	40.5	55.5	530	Peritectic	3(Na, Li)F·4ZrF_4 ss, LiF·NaF·4ZrF_4 ss, ZrF_4

Table II. Phase Transition Temperatures Observed on Cooling Molten Mixtures of LiF–ZrF_4 and LiF–NaF–ZrF_4

Composition, Mole %			Phase Transition Temperatures, ° C.			
LiF	NaF	ZrF_4	Liquidus	Liquid-solid boundary curve	Solidus	Solid state transitions
92		8			595	508,473
85		15	708		595	474
83		17	676		599	478
80		20			597	475
79		21	611		600	478
					600	475
77		23	640		592	477
75		25	658			493,478
73		27	658		575	478
71		29	637		580	450
70		30			568	478,470
69		31	602		582	473
66.7		33.3	587			
65		35	585			515
63		37	582		510	
60		40	567		512	
					505	482,468
53.8		46.2	529		515	
51		49			513	
49		51	526		516	
45		55	595	525	512	
42.5		57.5	617	528	514	
40		60				490,469
35		65	690	520	507	
30		70				469,462,435
25		75	770	525	513	
20		80				514,477,435
15		85	873	540		
50	45	5	630		600	
80	15	5	777		623	
42	49	9	618		605	
35	55	10	647		602	
40	50	10	610	608	603	
45	45	10	638		603	
60	30	10	712		625	
38	51	11			605	
40	49	11	616	609	604	
41	48	11	625	610	608	
46	40.5	13.5	658		625	
38	46.5	15.5			625	
30	52.5	17.5	660		624	
20	60	20	710		627	
15	63.75	21.25	764			
50	27	23			572	355
5	70	25	820		700	675,604
10	65	25	785		680	
15	60	25	749		675	575
20	55	25	703	690	595	
40	35	25	605			340
45	30	25	592			345
50	25	25		590		355
55	20	25	595			380,350
60	15	25	622			430,348
10	64	26	781			
5	68	27	810	627,620	585	
15	58	27	725	560		
35	38	27	597		490	355
40	33	27	582		455	353
45	28	27	577		453	353
50	23	27	576		444	356
20	52.5	27.5	670	565	552	340
25	47	28	630	512	435	340
35	37	28	575	480	440	348
40	32	28	567		443	350
45	27	28	566		455	350
48	24	28	580			350
50	22	28	568		475	356
5	66	29	787	618,611		
30	41	29	587	500	440	343
35	36	29	560	472	450	349
40	31	29	556		450	335
45	26	29	550	462	482	350
50	21	29			467	350
35	35	30	527	460	443	346
40	30	30	516		442	343
45	25	30	528	483	447	348
50	20	30	530	477	347	
			502		445	349
45	24.7	30.3	500	475	450	343
5	64	31	735	624,619		
30	39	31	510	467	455	344
35	34	31	453			
40	29	31	490			
45	24	31	490		450	345
50	19	31	510		445	346
55	13.3	31.7	542		452	345
35	33	32	455			
40	28	32	470		455	
45	23	32	500		455	
50	18	32	520	505	450	343
60	7.7	32.3	565		456	340
60	7.5	32.5	565	450		343
5	61.7	33.3	615	605,510	463	
10	56.7	33.3	635	490,438		
15	51.7	33.3		540,472	430	
20	46.7	33.3	545	450		427
25	41.7	33.3	485	440		
30	36.7	33.3	450		445	
35	31.7	33.3	460		430	
40	26.7	33.3		445	430	
			484	456	438	
45	21.7	33.3	510	447	435	
			512	450	438	
50	16.7	33.3	533	445		
55	11.7	33.3	551		445	
60	6.7	33.3	570	447		
29	35	36	445	435	433	
55	9	36	558			
35	28.6	36.4	480	430	425	
30	33.1	36.9	450		427	
25	38	37	430		425	
28	35	37	445	440	435	
29	34	37	452		430	
50	13	37	540			
17.5	44.7	37.8	450	446		
23	39	38	440		425	
24	38	38	438		423	
25	37	38	428		425	
26	36	38	440	425		
28	34	38	445		425	
29	33	38	440		427	
45	17	38	525	445		
23	38	39	443		421	
40	21	39	503		455	
22	38	40			428	
35	25	40	480		455	
28	30	42	458			
29	29	42	457			
28	29	43	453			
20	36.5	43.5	470	455		
28	28	44	452			
31	25	44	456			
26	29	45	457		450	
27	28	45	453			
28	27	45	450			
30	25	45	452		450	
32	23	45	460		450	
10	44.4	45.6	497		445	
28	26	46	450			
29	25	46	449			
28	25	47	453		450	
29	24	47	452		450	
10	41.5	48.5	494		445	
20	31	49		460	445	
30	21	49		453	450	
40	11	49	493	482	445	
15	33	52	497		497	437,425
10	32.5	57.5	576	512		432
20	22.5	57.5	588		463	458,438
30	12.5	57.5	610	582		438

Table III. Equilibrium Phase Transition Temperature Data Obtained from Quenched Specimens of LiF–ZrF_4 and LiF–NaF–ZrF_4

Composition, Mole %					
LiF	NaF	ZrF_4	Temp., °C.[a]	Phases[b] Above Temperature	Phases Below Temperature
92		8	784 ± 3	X	$X + L$
80		20	610 ± 3	X	$X + L$
			602 ± 3	$X + L$	$L + L_3Z$
79		21	604 ± 2	X	$X + L_3Z$
			598 ± 2	$X + L_3Z$	$L_3Z + L$
78		22	631 ± 3	X	$X + L_3Z$
			601 ± 3	$X + L_3Z$	$L_3Z + L$
75		25	649 ± 5	X	L_3Z
72.5		27.5	642 ± 3	X	$X + L_3Z$
69		31	592 ± 2	X	$X + L_2Z$
			571 ± 4	$X + L_2Z$	$L_2Z + L_3Z$
66.7		33.3	596 ± 3	X	L_2Z
63		37	577 ± 2	X	$X + L_2Z$
			510 ± 3	$X + L_2Z$	$L_2Z + L_3Z_4$
60		40	566 ± 3	X	$X + L_2Z$
			515 ± 3	$X + L_2Z$	$L_2Z + L_3Z_4$
			466 ± 2	$L_2Z + L_3Z_4$	$L_2Z + Z$
57.5		42.5	558 ± 3	X	$X + L_2Z$
			515 ± 3	$X + L_2Z$	$L_2Z + L_3Z_4$
			466 ± 2	$L_2Z + L_3Z_4$	$L_2Z + Z$
55		45	524 ± 3	X	$X + L_2Z$
			513 ± 3	$X + L_2Z$	$L_2Z + L_3Z_4$
			467 ± 2	$L_2Z + L_3Z_4$	$L_2Z + Z$
53.8		46.2	519 ± 2	X	$X + L_2Z$
			514 ± 2	$X + L_2Z$	$L_2Z + L_3Z_4$
52		48	519 ± 3	X	$X + L_2Z$
51		49	519 ± 2	X	$X + L_3Z_4$
			510 ± 2	$X + L_3Z_4$	$L_2Z + L_3Z_4$
50		50	525 ± 3	X	$X + L_3Z_4$
			513 ± 3	$X + L_3Z_4$	$L_2Z + L_3Z_4$
			467 ± 2	$L_2Z + L_3Z_4$	$L_2Z + Z$
49		51	519 ± 3	X	$X + L_3Z_4$
			514 ± 2	$X + L_3Z_4$	$L_3Z_4 + L_2Z$
47.5		52.5	533 ± 3	X	$X + L_3Z_4$
			515 ± 3	$X + L_3Z_4$	$L_3Z_4 + L_2Z$
			466 ± 2	$L_3Z_4 + L_2Z$	$L_2Z + Z$
42.9		57.1	621 ± 5	X	$X + Z$
			528 ± 5	$X + Z$	L_3Z_4
42.5		57.5	595 ± 2	X	$X + Z$
			524 ± 2	$X + Z$	L_3Z_4
			468 ± 2	L_3Z_4	$L_2Z + Z$
40		60	624 ± 3	X	$X + Z$
			520 ± 6	$X + Z$	$Z + L_3Z_4$
33.3		66.7	699 ± 6	X	$X + Z$
30		70	730 ± 6	X	$X + Z$
20		80	822 ± 3	X	$X + Z$
10		90	876 ± 3	X	$X + Z$
60	30	10	690 ± 3	X	$X + L$
			628 ± 3	$X + L$	$L + (N, L)_3Z$
65	20	15	700 ± 4	X	$X + L$
			554 ± 3	$X + L$	$X + L + (N, L)_3Z$
			539 ± 3	$X + (N, L)_3Z + L$	$L + (N, L)_3Z$
38	46.5	15.5	618 ± 3	X	$X + (N, L)_3Z + L$
			612 ± 3	$X + (N, L)_3Z + L$	$(N, L)_3Z + L$
20	60	20	693 ● 4	X	$X + (N, L)_3Z$
			612 ± 3	$X + (N, L)_3Z$	$(N, L)_3Z + L$
30	50	20	622 ± 3	$X + (N, L)_3Z$	$X + (N, L)_3Z + L$
			583 ± 3	$X + (N, L)_3Z + L$	$(N, L)_3Z + L$
5	70	25	812 ± 3	X	$X + (N, L)_3Z$
10	65	25	752 ± 3	X	$X + (N, L)_3Z$
20	55	25	692 ± 4	X	$X + (N, L)_3Z$
30	45	25	635 ± 2	X	$X + (N, L)_3Z$
			606 ± 3	$X + (N, L)_3Z$	$(N, L)_3Z$
35	40	25	610 ± 3	X	$X + (N, L)_3Z$
			594 ± 3	$X + (N, L)_3Z$	$(N, L)_3Z$
10	64	26	745 ± 4	X	$X + (N, L)_3Z$
15	58.5	26.5	692 ± 4	X	$X + (N, L)_3Z$
			588 ± 3	$X + (N, L)_3Z$	$(N, L)_3Z + \alpha\text{-}N_5Z_2$ ss
5	68	27	799 ± 7	X	$X + (N, L)_3Z$
30	41.5	28.5	506 ± 3	$X + (N, L)_3Z$	$X + (N, L)_3Z + \alpha\text{-}N_5Z_2$ ss
			444 ± 2	$X + (N, L)_3Z + \alpha\text{-}N_5Z_2$ ss	$\alpha\text{-}N_5Z_2$ ss $+ L_2Z$
5	66	29	794 ± 3	X	$X + (N, L)_3Z$

(*Continued on page 224*)

Table III. Equilibrium Phase Transition Temperature Data Obtained from Quenched Specimens of $LiF–ZrF_4$ and $LiF–NaF–ZrF_4$ (*Continued*)

Composition, Mole %					
LiF	NaF	ZrF_4	Temp., °C.[a]	Phases[b] Above Temperature	Phases Below Temperature
35	46	29	472 ± 3	$X + (L, N)_3Z$	$X + (L, N)_3Z + (N, L)_3Z$
40	31	29	550 ± 3	X	$X + (L, N)_3Z$
45	25	30	476 ± 3	X	$X + L_2Z$
			450 ± 2	$X + L_2Z$	$X + L_2Z + (N, L)_3Z$
45	24.5	30.5	476 ± 3	X	$X + L_2Z$
5	64	31	715 ± 3	X	$X + (N, L)_3Z$
			556 ± 2	$X + (N, L)_3Z$	$X + \alpha\text{-}N_5Z_2$ ss
			502 ± 2	$X + \alpha\text{-}N_5Z_2$ ss	$X + \alpha\text{-}N_5Z_2$ ss + $\alpha\text{-}N_2Z$
			483 ● 2	$X + \alpha\text{-}N_5Z_2$ ss + $\alpha\text{-}N_2Z$	$\alpha\text{-}N_5Z_2$ ss + $\alpha\text{-}N_2Z$
50	19	31	505 ± 4	X	$X + L_2Z$
			448 ± 3	$X + L_2Z$	$L_2Z + (L, N)_3Z$
35	33	32	448 ± 3	X	$X + L_2Z + (L, N)_3Z$
			434 ± 3	$X + L_2Z + (L, N)_3Z$	$L_2Z + (L, N)_3Z + \beta\text{-}N_2Z$
60	8	32	559 ± 3	X	$X + L_2Z$
			478 ± 3	$X + L_2Z$	$X + L_2Z + (L, N)_3Z$
			445 ± 2	$X + L_2Z + (L, N)_3Z$	$L_2Z + (L, N)_3Z + (N, L)_3Z$
5	61.7	33.3	611 ± 4	X	$X + \alpha\text{-}N_5Z_2$ ss
20	46.7	33.3	501 ± 3	X	$X + \alpha\text{-}N_5Z_2$ ss
25	41.7	33.3	475 ± 2	$X + (N, L)_3Z$	$X + (N, L)_3Z + \gamma\text{-}N_2Z$
			442 ± 2	$X + (N, L)_3Z + \alpha\text{-}N_2Z$	$\gamma\text{-}N_2Z + L_2Z$
45	21.7	33.3	501 ± 3	X	$X + L_2Z$
55	11.7	33.3	555 ± 3	X	$X + L_2Z$
			505 ± 3	$X + L_2Z$	$X + L_2Z + \alpha\text{-}N_5Z_2$ ss
60	6.7	33.3	568 ± 2	X	$X + L_2Z$
60	5	35	572 ± 3	X	$X + L_2Z$
55	9	36	560 ± 2	X	$X + L_2Z$
			455 ± 3	$X + L_2Z$	$L_2Z + N_7Z_6$
26	37	37	439 ± 2	X	$X + L_2Z + \gamma\text{-}N_2Z$
			436 ± 2	$X + L_2Z + \gamma\text{-}N_2Z$	$L_2Z + \gamma\text{-}N_2Z + N_3Z_2\text{-}N_7Z_6$ ss
45	17.5	37.5	524 ± 1	X	$X + L_2Z$
			452 ± 2	$X + L_2Z$	$L_2Z + N_7Z_6$
30	29.5	40.5	457 ± 2	X	$X + L_2Z$
			452 ± 3	$X + L_2Z$	$L_2Z + N_7Z_6$
40	17	43	496 ± 3	X	$X + L_2Z$
			450 ± 3	$X + L_2Z$	$L_2Z + N_7Z_6 + (N, L)_3Z_4$
28	26	44	450 ± 3	X	$X + N_7Z_6$
			447 ± 2	$X + N_7Z_6$	$N_7Z_6 + L_2Z + (N, L)_3Z_4$
31	25	44	455 ± 2	X	$X + L_2Z$
			451 ± 2	$X + L_2Z$	$X + L_2Z + N_7Z_6$
26	29	45	455 ± 2	X	$X + N_7Z_6$
			451 ± 2	$X + N_7Z_6$	$X + N_7Z_6 + L_2Z$
29	25	46	451 ± 2	X	$L_2Z + N_7Z_6$
31	23	46	455 ± 3	X	$X + L_2Z$
			450 ± 3	$X + L_2Z$	$X + L_2Z + (N, L)_3Z_4$
			445 ± 3	$X + L_2Z + (N, L)_3Z_4$	$L_2Z + N_7Z_6 + (N, L)_3Z_4$
41	13	46	500 ± 1	X	$X + L_2Z$
28	25	47	448 ± 2	X	$X + (N, L)_3Z_4$
			443 ± 3	$X + (N, L)_3Z_4$	$(N, L)_3Z_4 + L_2Z$
20	30	50	473 ± 3	X	$X + (N, L)_3Z_4$
			455 ± 3	$X + (N, L)_3Z_4$	$X + (N, L)_3Z_4 + N_7Z_6$
			440 ± 3	$X + (N, L)_3Z_4 + N_7Z_6$	$(N, L)_3Z_4 + N_7Z_6$
25	25	50	471 ± 2	X	$X + (N, L)_3Z_4$
			451 ± 2	$X + (N, L)_3Z_4$	$X + (N, L)_3Z_4 + L_2Z$
			442 ± 2	$X + (N, L)_3Z_4 + L_2Z$	$(N, L)_3Z_4 + L_2Z$
30	20	50	479 ± 2	X	$X + LNZ_4$
			464 ± 2	$X + LNZ_4$	$X + (N, L)_3Z_4$
35	15	50	484 ± 2	X	$X + (L, N)_3Z_4$
			470 ± 2	$X + (L, N)_3Z_4$	$X + (L, N)_3Z_4 + L_2Z$
			456 ± 3	$X + (L, N)_3Z_4 + L_2Z$	$(L, N)_3Z_4 + L_2Z$
15	34	51	472 ± 3	X	$X + (N, L)_3Z_4$
			449 ± 2	$X + (N, L)_3Z_4$	$X + (N, L)_3Z_4 + N_7Z_6$
10	36.5	53.5	514 ± 2	X	$X + Z$
			510 ± 2	$X + Z$	$X + (N, L)_3Z_4$
			464 ± 3	$X + (N, L)_3Z_4$	$X + (N, L)_3Z_4 + N_7Z_6$
			451 ± 2	$X + (N, L)_3Z_4 + N_7Z_6$	$(N, L)_3Z_4 + N_7Z_6$
18	27	55	473 ± 2	$X + LNZ_4$	$(L, N)_3Z_4$
10	32.8	57.2	517 ± 3	X	$X + LNZ_4$
			496 ± 3	$X + LNZ_4$	$X + (N, L)_3Z_4$
			476 ± 3	$X + (N, L)_3Z_4$	$(N, L)_3Z_4$

(*Continued on page 225*)

Table III. Equilibrium Phase Transition Temperature Data Obtained from Quenched Specimens of $LiF-ZrF_4$ and $LiF-NaF-ZrF_4$ (*Continued*)

Composition, Mole %					
LiF	NaF	ZrF_4	Temp., ° C.[a]	Phases[b] Above Temperature	Phases Below Temperature
10	32.5	57.5	544 ± 5	X	$X + Z$
			514 ± 5	$X + Z$	$X + LNZ_4$
			484 ± 3	$X + LNZ_4$	$LNZ_4 + (N, L)_3Z_4$
26	16.8	57.2	538 ± 3	X	$X + Z$
			481 ± 3	$X + Z$	$Z + LNZ_4$
			465 ± 3	$Z + LNZ_4$	$(N, L)_3Z_4$
			451 ± 2	$(N, L)_3Z_4$	$(N, L)_3Z_4 + Z + L_2Z$
30	12.8	57.2	562 ± 3	X	$X + Z$
			504 ± 3	$X + Z$	$X + Z + (L, N)_3Z_4$
			491 ± 3	$X + Z + (L, N)_3Z_4$	$X + (L, N)_3Z_4$
			484 ± 3	$X + (L, N)_3Z_4$	$(L, N)_3Z_4$
35	7.5	57.5	562 ± 3	X	$X + Z$
			493 ± 3	$X + Z$	$X + Z + (L, N)_3Z_4$
			462 ± 3	$X + Z + (L, N)_3Z_4$	$X + (L, N)_3Z_4 + L_2Z$
			449 ± 2	$X + (L, N)_3Z_4 + L_2Z$	$(L, N)_3Z_4 + L_2Z + Z$
10	30	60	576 ± 3	X	$X + Z$
			500 ± 3	$X + Z$	$X + LNZ_4$
			479 ± 3	$X + LNZ_4$	$LNZ_4 + (N, L)_3Z_4$
20	20	60	590 ± 3	X	$X + Z$
			482 ± 2	$X + Z$	$X + LNZ_4$
			449 ± 2	$X + LNZ_4$	$LNZ_4 + (N, L)_3Z_4$
			445 ± 2	$LNZ_4 + (N, L)_3Z_4$	$LNZ_4 + (N, L)_3Z_4 + L_2Z$
10	27	63	608 ± 3	X	$X + Z$
10	25	65	645 ± 3	X	$X + Z$
			504 ± 3	$X + Z$	$X + LNZ_4 + Z$
			498 ± 3	$X + LNZ_4 + Z$	$X + LNZ_4$
			491 ± 4	$X + LNZ_4$	$X + LNZ_4 + (N, L)_3Z_4$
			442 ± 3	$X + LNZ_4 + (N, L)_3Z_4$	$LNZ_4 + (N, L)_3Z_4$
25	10	65	632 ± 4	X	$X + Z$
			472 ± 3	$X + Z$	$X + Z + (N, L)_3Z_4$
			466 ± 3	$X + Z + (N, L)_3Z_4$	$X + Z + LNZ_4$
			460 ± 3	$X + Z + LNZ_4$	$LNZ_4 + Z + L_2Z$
4	29.3	66.7	650 ± 3	X	$X + Z$
			524 ± 3	$X + Z$	$X + Z + LNZ_4$
			500 ± 3	$X + Z + LNZ_4$	$Z + LNZ_4 + (L, N)_3Z_4$
6.3	27	66.7	635 ± 5	X	$X + Z$
			514 ± 3	$X + Z$	$X + LNZ_4$
			470 ± 3	$X + LNZ_4$	LNZ_4
9	24.3	66.7	650 ± 3	X	$X + Z$
			505 ± 3	$X + Z$	$X + LNZ_4$
			470 ± 3	$X + LNZ_4$	LNZ_4
14	19.3	66.7	650 ± 3	X	$X + Z$
			485 ± 3	$X + Z$	$X + LNZ_4$
16.7	16.6	66.7	646 ± 4	X	$X + Z$
			478 ± 3	$X + Z$	LNZ_4
15	15	70	484 ± 2	$X + Z$	$Z + LNZ_4$
12.5	12.5	75	652 ± 4	X	$X + Z$
			484 ± 2	$X + Z$	$Z + LNZ_4$
10	10	80	481 ± 3	$X + Z$	$Z + LNZ_4$

[a] Precision limits indicate temperature intervals existing between container segments during annealing period. [b] Symbols designating phases identified in quenched samples are coded as follows:

X = liquid
L = LiF
L_3Z = $3LiF \cdot ZrF_4$
L_2Z = $2LiF \cdot ZrF_4$
L_3Z_4 = $3LiF \cdot 4ZrF_4$
Z = ZrF_4
$(N, L)_3Z$ = $3NaF \cdot ZrF_4$ solid solution, a fraction of the Na^+ sites occupied by Li^+
$(L, N)_3Z$ = β-$3LiF \cdot ZrF_4$ solid solution, a fraction of the Li^+ sites occupied by Na^+
α-N_5Z_2 ss = α-$5NaF \cdot 2ZrF_4$ solid solution, containing excess Na^+ and/or Li^+
N_2Z = $2NaF \cdot ZrF_4$
N_3Z_2 = $3NaF \cdot 2ZrF_4$
N_7Z_6 = $7NaF \cdot 6ZrF_4$
$(N, L)_3Z_4$ = $3NaF \cdot 4ZrF_4$ solid solution, a fraction of the Na^+ sites occupied by Li^+
$(L, N)_3Z_4$ = $3LiF \cdot 4ZrF_4$ solid solution, a fraction of the Li^+ sites occupied by Na^+
LNZ_4 = $LiF \cdot NaF \cdot 4ZrF_4$ or solid solutions of this compound in which a fraction of the Li^+ sites are occupied by Na^+

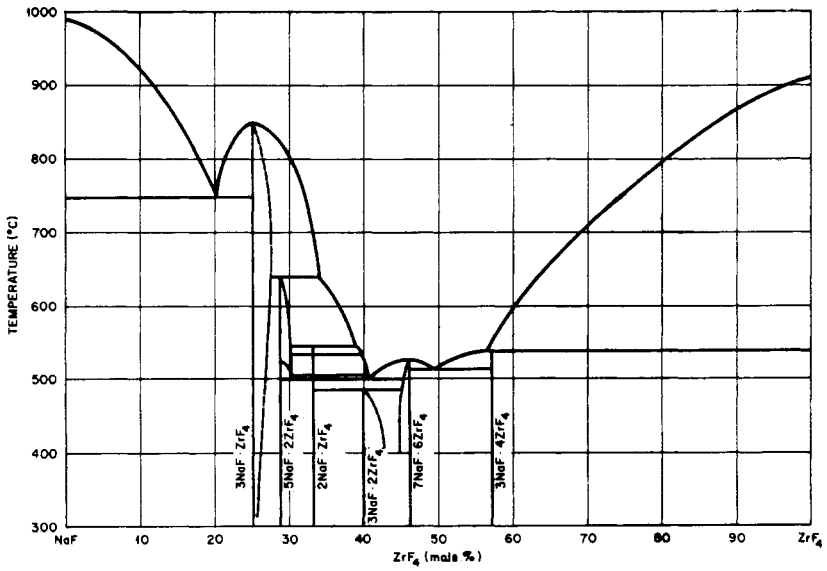

Figure 3. The system $NaF-ZrF_4$

lithium and sodium ions exchange sites in the intermediate compounds which crystallize from $LiF-NaF-ZrF_4$ melts gives rise to complex phase behavior, particularly in the solid-state reactions observed in this system. The complexity is compounded by the interchangeability of Li^+ and Na^+ ions in some of the crystalline phases, and in that even some of the limiting solid phases—namely, $3NaF \cdot ZrF_4$, $5NaF \cdot 2ZrF_4$, and $7NaF \cdot 6ZrF_4$ (Figure 3)—exhibit compositional variability. These phenomena are displayed in the phase diagram in three classes of solid solutions: compositionally variable solids containing a single alkali fluoride—i.e., $NaF-ZrF_4$ phases; limited solid solutions in which Li^+ is substituted for some of the sites in the first class of solids, for which Li^+-Na^+ exchange gives rise to single phase compositions at a given isotherm and are representable by areas—e.g., solids such as $3(Na,Li)F \cdot ZrF_4$–$5(Na,Li)F \cdot 2ZrF_4$, $3(Li,Na)F \cdot ZrF_4$—or by lines, as in $LiF \cdot NaF \cdot 4ZrF_4$ and $3LiF \cdot ZrF_4$ solid solutions; and continuous solid solutions formed from isomorphous phases—e.g., $3LiF \cdot 4ZrF_4$–$3NaF \cdot 4ZrF_4$.

Optical properties and x-ray diffraction data for the pure compounds isolated in the ternary system and the limiting binary systems are given in Table IV. These data summarize the total identification data for the complex fluorides formed from LiF, NaF, and ZrF_4. Future insights into the perspectives on $LiF-NaF-ZrF_4$ phase behavior should be obtained from structural studies of the complex solid species described here.

Several experimental factors were encountered in the investigation of the $LiF-NaF-ZrF_4$ system which prevented the elucidation of solid phase equilibria in as much detail as has been customary in previous investigations of fluoride ternary systems reported from this Laboratory. Chiefly, these are: (1) the formidable number of analyses and identifications required to determine the composition-temperature boundaries differentiating several partial solid solutions, particularly in the compositions near $3NaF \cdot ZrF_4$, $5NaF \cdot 2ZrF_4$, and $2NaF \cdot ZrF_4$, (2) the great tendency of $LiF-NaF-ZrF_4$ melts with concentrations of ZrF_4 in excess of 40 mole % to become hydrolyzed by traces of contami-

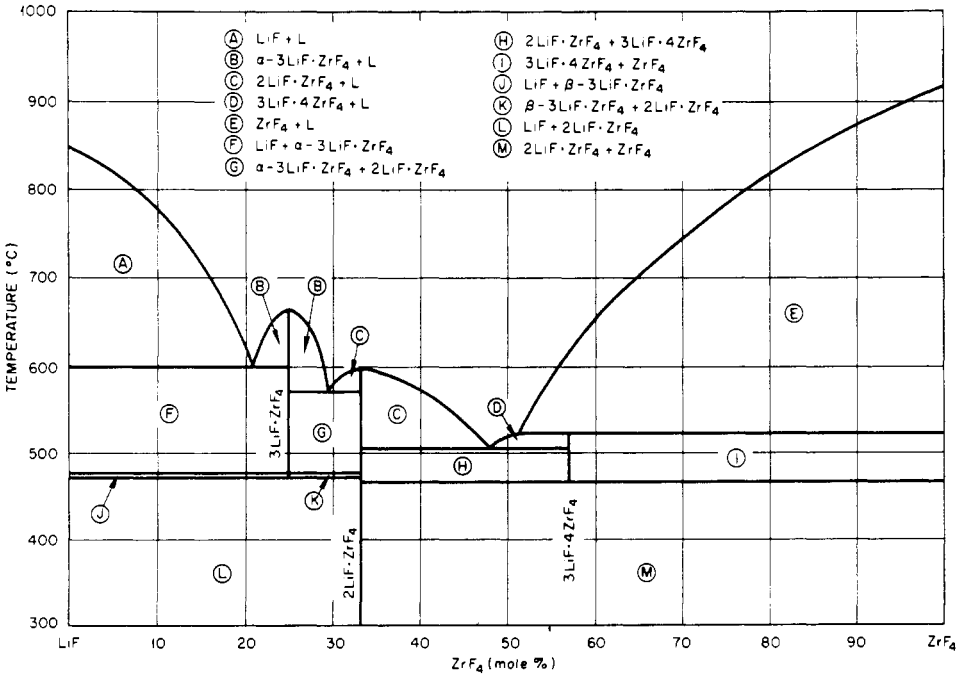

Figure 4. The system $LiF-ZrF_4$

Table IV. Optical Properties and X-Ray Data[a] for Crystal Phases in the System LiF–NaF–ZrF_4

Compound	Optical Properties	Crystal Structure
LiF	Isotropic, $N = 1.392$ (*17*)	Fcc, $a_o = 4.0270$ (*18*)
NaF	Isotropic, $N = 1.326$ (*15*)	Fcc, $a_o = 4.6344$ (*18*)
ZrF_4	Biaxial negative, $N_\alpha = 1.560$, $N_\beta = 1.598$, $N_\gamma = 1.606$ $2V = 52°$	Monoclinic, $a_o = 4.6344$ $b_o = 9.89A$, $c_o = 7.66A$ $\beta = 126°9'$ (*5*)
$2LiF \cdot ZrF_4$	Uniaxial positive, $N_\omega = 1.468$, $N = 1.478$	Hexagonal, $P\bar{3}1m$, $a = 4.98A$, $c = 4.66A$ (*12*)
$3NaF \cdot ZrF_4$	$N = 1.470$ birefringence very low	Tetragonal $I\,4/mmm$ $a_o = 5.31$, $c_o = 10.50$ (*10*)
$7NaF \cdot 6ZrF_4$	Uniaxial negative, $N_\omega = 1.508$, $N_\epsilon = 1.500$	Rhombohedral, $R\bar{3}$ $a_o = 8.565A$, $\alpha = 107°21'$ (*1*)

α-$3LiF \cdot ZrF_4$ (*20*)
Optical properties: isotropic, $N = 1.420$

d (A)	I/I_1	d (A)	I/I_1
7.2	15	3.15	60
6.42	15	2.84	40
5.68	15	2.63	20
4.58	100	2.535	10
3.75	15	2.361	15
3.68	12	2.20	10
3.43	15	2.047	65
3.24	30	1.847	20

β-$3LiF \cdot ZrF_4$
Optical properties: biaxial negative, $N_\alpha = 1.445$, $N_\gamma = 1.465$, $2V = 30°$

5.49	55	2.07	100
5.40	35	1.94	20
4.88	50	1.82	25
3.67	25	1.80	12
3.43	5	1.78	12
2.91	15	1.65	5
2.79	8	1.59	5
2.67	15	1.57	5
2.40	5		

$3LiF \cdot 4ZrF_4$
Optical properties: biaxial positive, $N_\alpha = 1.463$, $N_\gamma = 1.473$, $2V = 25°$

6.11	25	2.615	15
5.24	35	2.303	10
4.90	15	2.248	10
4.21	30	2.227	5
4.00	10	2.194	85
3.90	95	2.159	15
3.77	20	2.043	10
3.69	5	2.130	35
3.33	60	1.947	35
3.29	20	1.912	20
3.26	20	1.883	10
3.16	100	1.721	10

$LiF \cdot 4ZrF_4$ (metastable)
Optical properties: uniaxial positive, $N_\omega = 1.582$, $N_\epsilon = 1.588$

5.61	25	2.080	5
3.95	100	1.934	10
3.88	100	1.92	90
3.54	100	1.864	50
3.43	10	1.842	5
2.796	20	1.768	10
2.763	20	1.719	65
2.614	70	1.680	20
2.501	10	1.481	5

α-$5NaF \cdot 2ZrF_4$
Optical properties: uniaxial positive, $N_\omega = 1.396$, $N_\epsilon = 1.400$

5.45	10	2.206	10
5.15	55	2.169	5
4.73	25	2.088	10
4.06	15	2.038	15
3.83	5	1.995	10
3.72	40	1.951	7
3.48	15	1.890	100
3.43	5	1.847	5
3.15	5	1.812	5
3.09	100	1.776	10
2.839	5	1.711	5
2.682	10	1.688	5
2.593	5	1.630	5
2.327	10	1.611	45
2.237	5		

β-$5NaF \cdot 2ZrF_4$ (*3, 11*)
Optical properties: biaxial negative, $N_\alpha = 1.393$, $N_\gamma = 1.402$, $2V = 40°$

5.76	25	2.416	10
5.06	15	2.344	15
4.97	100	2.302	5
4.68	15	2.206	10
4.48	45	2.123	10
4.37	25	2.090	5
4.18	65	2.029	80
3.61	20	1.977	20
3.45	5	1.899	70
3.38	5	1.863	5
3.29	25	1.840	25
3.19	10	1.807	10
3.11	100	1.666	10
3.05	100	1.648	10
2.866	15	1.590	10
2.844	15	1.578	10
2.485	5		

α-$2NaF \cdot ZrF_4$
Optical properties: biaxial negative, $N_\alpha = 1.412$, $N_\gamma = 1.419$, $2V = 75°$

5.72	20	2.216	20
5.47	80	2.043	20
5.38	50	1.912	100
3.78	80	1.897	80
3.31	20	1.793	20
3.11	100	1.645	20
2.675	20	1.617	50
2.410	20	1.557	10

β-$2NaF \cdot ZrF_4$
Optical properties: uniaxial positive, $N_\omega = 1.376$, $N_\epsilon = 1.386$

5.12	100	2.557	10
4.80	10	2.550	10
4.55	100	2.475	40
4.00	5	2.275	30
3.89	10	2.221	30
3.82	10	2.085	10
3.60	90	1.894	100
3.24	25	1.799	30
3.12	30	1.708	60
3.04	10	1.608	5
2.95	40	1.543	20
2.893	100		

γ-$2NaF \cdot ZrF_4$
Optical properties: biaxial positive, $N_\alpha = 1.408$, $N_\gamma = 1.412$, $2V = 75°$

7.97	35	2.564	20
5.54	15	2.398	15
4.12	80	2.361	15
4.88	65	2.327	15
4.48	15	2.034	20
4.33	20	1.979	15
4.00	70	1.935	20
3.83	70	1.912	50
3.25	100	1.796	15
3.12	50	1.751	10
3.04	40	1.711	20
2.89	15	1.619	10
2.759	25	1.596	20
2.666	20	1.574	15

(*Continued on page 228*)

Table IV. Optical Properties and X-Ray Data[a] for Crystal Phases in the System LiF–NaF–ZrF_4 (*Continued*)

d (A)	I/I_1	d (A)	I/I_1

δ-$2NaF \cdot ZrF_4$

Optical properties: biaxial negative, $N_\alpha = 1.420$, $N_\gamma = 1.429$, $2V > 70°$

4.98	100	3.36	60
4.37	50	3.16	40
4.19	80	3.07	80
3.96	50	2.839	70
3.45	50	1.843	50

$3NaF \cdot 2ZrF_4$

Optical properties: $N = 1.470$, birefringence very low

3.3	100
2.72	15
1.92	100
1.91	100
1.63	50

$NaF \cdot ZrF_4$ (metastable)

Optical properties: uniaxial positive, $N_\omega = 1.417$, $N_\epsilon = 1.446$

5.57	30	2.05	5
3.37	40	2.02	15
3.96	30	2.00	5
3.86	100	1.99	10
3.01	15	1.86	15
2.86	10	1.84	7
2.75	7	1.70	20
2.72	7	1.65	20
2.51	7	1.63	12
2.28	25	1.61	7
2.21	20	1.56	10
2.09	30		

$3NaF \cdot 4ZrF_4$

Optical properties: biaxial positive, $N_\alpha = 1.420$, $N_\gamma = 1.432$, $2V = 30°$

7.56	15	3.39	35
7.42	45	3.36	60
5.47	15	2.630	15
4.15	100	2.074	75
3.78	20	1.935	12
3.74	20	1.766	50
3.42	25	1.506	25

$NaF \cdot LiF \cdot 4ZrF_4$

Optical properties: Pure compound – biaxial positive, $N_\alpha = 1.486$, $N_\gamma = 1.514$, $2V = 50$ to $70°$

Limiting solid solution – biaxial positive, $N_\alpha = 1.470$, $N_\gamma = 1.498$, $2V = 50$ to $70°$

7.05	40	2.568	10
5.16	10	2.543	10
4.93	30	2.361	5
4.15	10	2.186	10
4.00	80	2.051	10
3.77	5	2.031	5
3.38	100	1.918	15
3.29	30	1.773	15
3.16	10	1.740	5
3.03	10	1.727	10
2.60	5	1.688	10

$3LiF \cdot 4ZrF_4$–$3NaF \cdot 4ZrF_4$ Solid Solutions

Refractive Indices as Functions of LiF Concentration

LiF Concentration, Mole %	N_α, Theoretical	N_α, Measured	N_γ, Theoretical	N_γ, Measured
0	1.420		1.432	
5	1.425		1.437	
10	1.430	1.428	1.442	1.440
15	1.436		1.447	
20	1.441	1.436	1.452	1.446
25	1.446	1.446	1.457	1.456
30	1.451		1.462	
35	1.456	1.456	1.467	1.464
40	1.462		1.472	
42.8	1.463		1.473	

[a] Indexed powder patterns are omitted from this table. Powder patterns for those phases as well as some of those listed below may be found in the ASTM X-Ray Diffraction Card File, numbers 10-116, 10-117, 10-118, 10-119, 10-165, 10-166, 10-167, 10-170, 10-176, 10-177, and 12-562.

nant moisture, (3) the hygroscopic character of the compounds $3LiF \cdot 4ZrF_4$ and $3NaF \cdot 4ZrF_4$, and (4) the volatility of ZrF_4 at temperatures in excess of 750° C. In combination, the effect of the three factors was to reduce the useful body of data acquired from mixtures containing ZrF_4 in high concentrations. The solid phases $3LiF \cdot 4ZrF_4$ and $3NaF \cdot 4ZrF_4$ apparently tend to adsorb moisture from the atmosphere at room temperature, for annealed and quenched specimens containing these phases were generally contaminated with small amounts of oxyfluoride phases of high refractive index, even though specimens examined microscopically before annealing appeared to be free of contaminating oxyfluorides or ZrO_2. The 3-to-4 compounds are unique among the intermediate compounds in the limiting binary systems in being curiously hygroscopic and in possessing abnormally low refractive indices, both qualities were adduced to be indicative of quite open structures in the crystalline solids. As gradual hydrolysis of the molten fluoride mixtures proceeds, crystallization in the $3LiF \cdot 4ZrF_4$–$3NaF \cdot 4ZrF_4$ primary phase field is affected such that tie lines are turned to indicate that the solid phase is richer in Na^+ than expected. This means that as contamination of specimens by hydrolysis products increases, contaminants formed are not simply oxyfluorides of zirconium but contain lithium as well. The contaminant oxyfluorides, occasionally observed in annealed and quenched samples, are observed in petrographic examination rather than in x-ray diffraction analysis. The oxyfluorides observed in this study occur as minute hexagonal platelets which are generally uniaxial with refractive indices, $N_\epsilon = 1.506$ and $N_\omega = 1.580$. When the hydrolysis reaction has proceeded sufficiently to produce phases detectable in x-ray powder patterns, ZrO_2 is detected rather than the smaller amounts of contaminating oxyfluorides. Nevertheless, contamination of melts by oxyfluorides near 50 to 55 mole % ZrF_4 and at the liquidus temperatures was sometimes sufficiently large to alter the nominal composition to the extent that deviations in the phase transition temperatures of 15° to 40° were observed.

System LiF–ZrF_4. Of the binary systems of ZrF_4 with the alkali fluorides, the system LiF–ZrF_4 (Figure 4) is the simplest. Solid solutions do not occur, and only 3 solid compounds are formed from equilibrium reactions of LiF and ZrF_4, the congruently melting compounds $3LiF \cdot ZrF_4$ and $2LiF \cdot ZrF_4$ and the incongruently melting compound $3LiF \cdot 4ZrF_4$. Of the three compounds, only $3LiF \cdot ZrF_4$ undergoes a polymorphic transition, inverting at 475° C., then decomposing to LiF and $2LiF \cdot ZrF_4$ on cooling to temperatures below 460° C. The crystal structure of only the intermediate phase, $2LiF \cdot ZrF_4$ (Table IV), has been determined (*12*). Both compounds, $3LiF \cdot ZrF_4$ and $3LiF \cdot 4ZrF_4$, exhibit lower temperature limits of stability; they decompose on cooling, the former to $2LiF \cdot ZrF_4$ and LiF, the latter to $2LiF \cdot ZrF_4$ and ZrF_4. Thus, the equilibrium solid phases in the system LiF–ZrF_4 below 460° C. are LiF, $2LiF \cdot ZrF_4$, and monoclinic ZrF_4. The LiF–ZrF_4 system is distinguished from other alkali fluoride–ZrF_4 binary systems by the large domain of the $2MF \cdot ZrF_4$ primary phase, $2LiF \cdot ZrF_4$, between 29.5 and 48 mole % ZrF_4, and the fact that no solid equilibrium compound occurs in the mid-composition region, though in other alkali fluoride–MF_4 binary systems where M^-/M^{+4} radius ratios are either larger or smaller than for Li^+/Zr^{+4} (0.88) $7MF \cdot 6MF_4$ compounds are found as equilibrium phases.

Two nonequilibrium crystalline phases, $LiF \cdot 4ZrF_4$ and a cubic form of ZrF_4 (Table IV), were encountered in the study of LiF–ZrF_4 equilibria, particularly in those samples which were cooled rapidly. It is possible that either or both of these phases are stabilized like cubic $3KF \cdot UF_4$ (*21*) by minute amounts of oxide ion. If so, however, very little oxide is required because the refractive indices in each of the two cases are so close to those of the pure fluorides

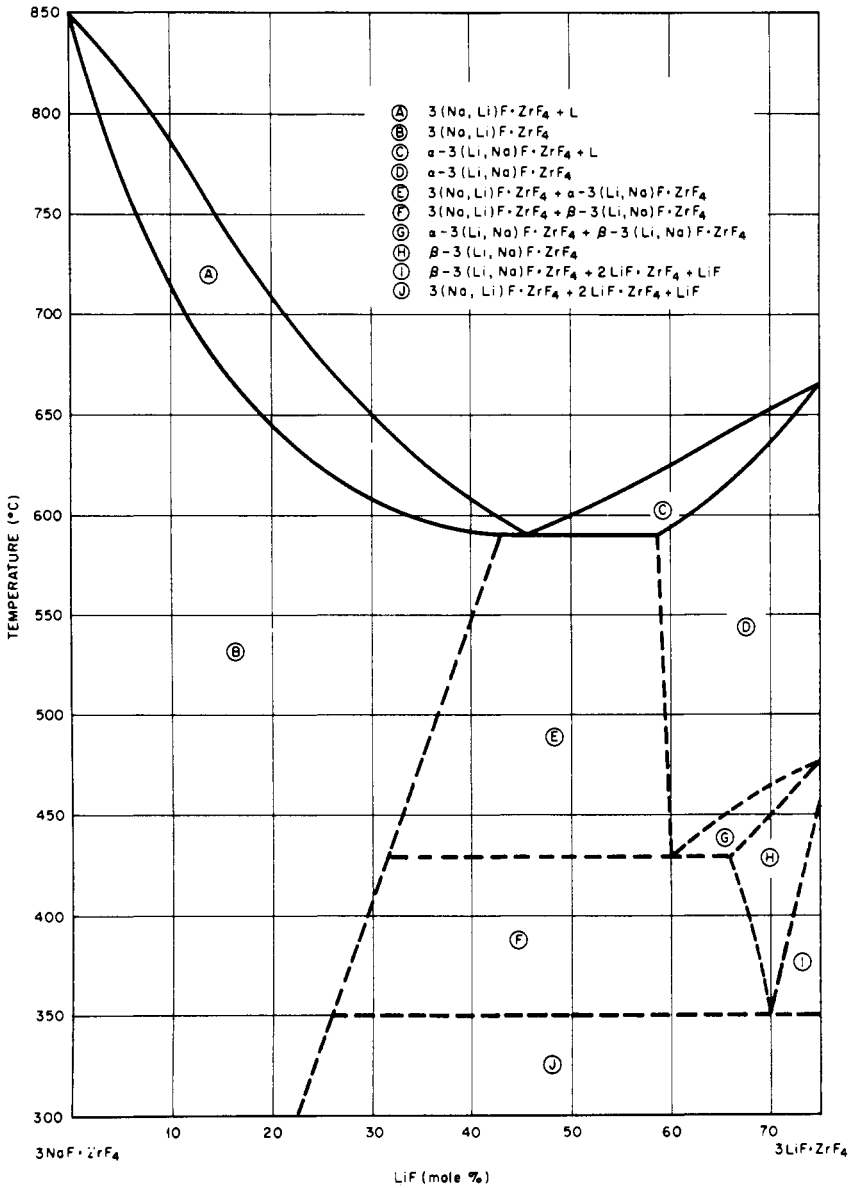

Figure 5. The section $3NaF \cdot ZrF_4$–$3LiF \cdot ZrF_4$

that the presence of hydrolysis products cannot be inferred.

System LiF–NaF–ZrF_4. Crystallization reactions occurring in the system LiF–NaF–ZrF_4 were discussed in general by Ricci in an earlier interim report (*16*). Qualitatively, the principal new information obtained for the system since that time pertains to the ternary compound $LiF \cdot NaF \cdot 4ZrF_4$, which was recently discovered. Additional data on other parts of the system have required some change in positions of boundary curves and invariant points.

Subsystem LiF–NaF–$3NaF \cdot ZrF_4$–$3LiF \cdot ZrF_4$. The compounds $3LiF \cdot ZrF_4$ and $3NaF \cdot ZrF_4$, both congruently melting, are partly miscible in the solid state and form a quasi-binary system, described in Figure 5. A quasi-binary system is formed from LiF and $3NaF \cdot ZrF_4$, having a minimum liquidus temperature of 625° C. for the composition 38–46.5–15.5 (LiF–NaF–ZrF_4, mole %). Liquids having compositions in the subsystem LiF–NaF–$3NaF \cdot ZrF_4$ freeze to 3 solids at the eutectic temperature, 604° C.

The LiF–NaF–$3NaF \cdot ZrF_4$–$3LiF \cdot ZrF_4$ ternary subsystem is itself comprised of two independent ternary subsystems, LiF–NaF–$3NaF \cdot ZrF_4$ and LiF–$3NaF \cdot ZrF_4$–$3LiF \cdot ZrF_4$. The absence of solid-state miscibility in the former enables all mixtures to become partially molten above 604° C.; liquidus of compositions near the quasi-binary system $3LiF \cdot ZrF_4$–$3LiF \cdot ZrF_4$, however, freeze above the 572° C. eutectic temperature because they do not precipitate the end member solids.

Subsystem $3NaF \cdot ZrF_4$–$7NaF \cdot 6ZrF_4$–$2LiF \cdot ZrF_4$–$3LiF \cdot ZrF_4$. The bounding quasi-binary system, $3NaF \cdot ZrF_4$–$3LiF \cdot ZrF_4$, of this subsystem is shown in Figure 5. The bounding quasi-binary system, $7NaF \cdot 6ZrF_4$–$2LiF \cdot ZrF_4$, is a simple eutectic system (Figure 6), the components of which melt congruently and show no inversions or decompositions. The subsystem contains two eutectic points. At one of these the liquids freeze to the solid phases, $3NaF \cdot ZrF_4$ ss (solid solution),

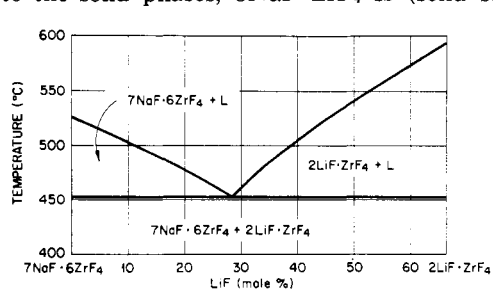

Figure 6. The quasi-binary system $7NaF \cdot 6ZrF_4$–$2LiF \cdot ZrF_4$

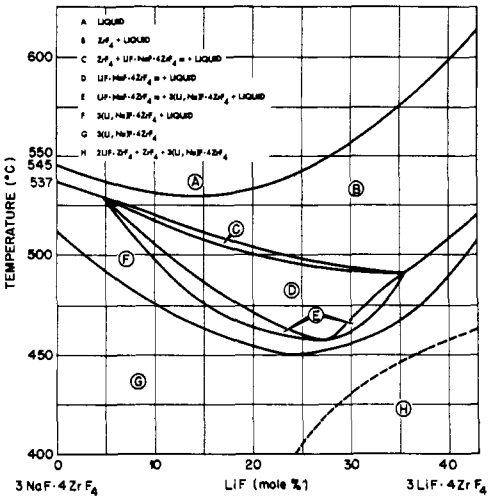

Figure 7. The section $3NaF \cdot 4ZrF_4$–$3LiF \cdot 4ZrF_4$

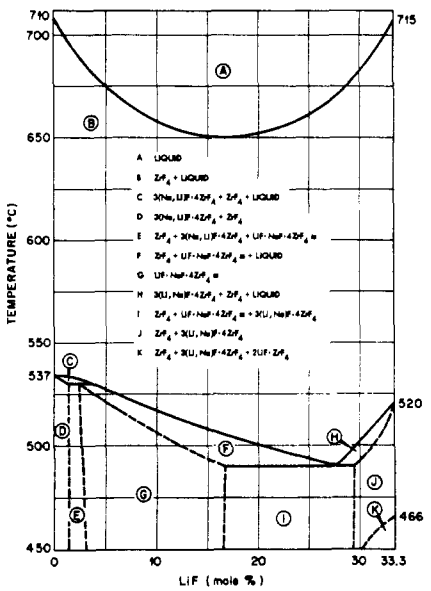

Figure 8. The section at 66.7 mole % ZrF_4

$3LiF \cdot ZrF_4$ ss, and $2LiF \cdot ZrF_4$. At the other the liquids freeze to the solid phases γ-$2NaF \cdot ZrF_4$, $7NaF \cdot 6ZrF_4$, and $2LiF \cdot ZrF_4$. Three forms of $2NaF \cdot ZrF_4$ participate in reactions at the liquidus in this system. The temperatures in the inversion $\alpha \rightleftarrows \beta \rightleftarrows \gamma$ $2NaF \cdot ZrF_4$ are, respectively, 533° and 505° C.

Subsystem $7NaF \cdot 6ZrF_4$–ZrF_4–$2LiF \cdot ZrF_4$. Crystallization reactions in this subsystem are rather complex, primarily because of the ease with which lithium and sodium ions may replace each other in the $3(Na, Li)F \cdot 4ZrF_4$ solid solution and in $LiF \cdot NaF \cdot 4ZrF_4$. The effects of these substitutions are readily seen in the solid solutions behavior involving the two 3-to-4 compounds, $3LiF \cdot 4ZrF_4$ and $3NaF \cdot 4ZrF_4$ (Figure 7), as well as in the solid solution behavior involving the incongruently melting compound $LiF \cdot NaF \cdot 4ZrF_4$. Complete miscibility in the solid state occurs between the 3-to-4 compounds while $LiF \cdot NaF \cdot 4ZrF_4$ forms partial solid solutions with the hypothetical compound $NaF \cdot 2ZrF_4$. Phase behavior between 3-to-4 compounds is further complicated by the instability of $3LiF \cdot 4ZrF_4$ at low temperatures. These compounds, as well as the ternary compound $LiF \cdot NaF \cdot 4ZrF_4$, display low crystal symmetry. Single crystals of the phases have not yet been obtained.

As indicated by the observed composition of the ternary compound as a single phase, by the maximum change in refractive indices, and by the maximum shift in the x-ray diffraction pattern, the compound $NaF \cdot LiF \cdot 4ZrF_4$ can take into solid solution "$NaF \cdot 2ZrF_4$" up to a limiting composition of approximately 27NaF, 6.3LiF, 66.7ZrF_4, in mole %. At this limiting composition the refractive indices are $N_\alpha = 1.470$, $N_\gamma = 1.498$. The polythermal section of the ternary system at the 66.7 mole % ZrF_4 level, which includes the compound $NaF \cdot LiF \cdot 4ZrF_4$ and its solid solution limit, is shown in Figure 8.

In equilibrium freezing in the subsystem, only liquids of compositions roughly below 50 mole % ZrF_4 reach the eutectic to produce three solids; liquids of compositions with more than 50 mole % ZrF_4 solidify to two solids before reaching the 446° C. eutectic in equilibrium freezing. Numerous mixtures in this subsystem can experience nonequilibrium freezing and produce eutectic reactions by crystallization reactions which depart from those described by Figure 1.

In LiF–NaF–ZrF_4 liquids rich in ZrF_4, association forces are exerted with considerable strength. Even for mixtures in which ZrF_4 is the primary phase, these forces are so pronounced that the liquidus surface displays slight concavity (Figure 1).

ACKNOWLEDGMENT

The study of these systems has been aided by many individuals to whom we are grateful, but we are especially indebted for help, advice, and encouragement to F.F. Blankenship, R.E. Moore, T.N. McVay, C.J. Barton, J.E. Ricci, and W.R. Grimes.

LITERATURE CITED

(1) Agron, P.A., Ellison, R.D., *J. Phys. Chem.* **63**, 2076 (1959).
(2) Barton, C.J., Friedman, H.A., *et al, J. Am. Ceram. Soc.* **41**, 63 (1958).
(3) Barton, C.J., Grimes, W.R., *et al, J. Phys. Chem.* **62**, 665 (1958).
(4) Bergman, A.G., Dergunov, E.P., *Compt. rend. acad. sci. USSR* **31**, 753 (1941).
(5) Burbank, R.D., Bensey J.N., Jr., *U.S. At. Energy Comm. Rept.* **K-1280**, 1956.
(6) Cathers, G.I., *et al, Proc. U.N. Intern. Conf. Peaceful Uses At. Energy, 2nd, Geneva, 1958* **17**, 473 (1959),P/535.
(7) Friedman, H.A., Hebert, G.M., Thoma, R.E., "Thermal Analysis and Gradient Quenching Apparatus and Techniques for the Investigation of Fused Salt Phase Equilibria" **ORNL-3373**, Dec. 18, 1962.
(8) Grimes, W.R., *et al*, "ANP Program Progr. Rept. June 10, 1955," pp. 51–5, **ORNL-1896** (declassified)
(9) Grimes, W.R., Cuneo, D.R., in "Reactor Handbook," C.R. Tipton, Jr., Ed., 2nd ed., Vol. I, pp. 425–73, Interscience, New York, 1960.
(10) Hampson, G.C., Pauling L., *J. Am. Chem. Soc.* **60**, 2702 (1938).
(11) Herak, R.M., Manojlovic, Lj. M., Malcic, S.S., *Bull. Boris Kidric Inst. Nucl. Sci.* **14**, 21 (1963).
(12) Hoppe, R. Dahne, W., *Naturwissenschaften* **17**, 397 (1960).
(13) Insley, H., Thoma, R.E., Friedman, H.A., Weaver, C.F., *Bull. Soc. Franc. Ceram.* **48**, 57 (1960).
(14) Lawrowski, S., Ed., *Reactor Fuel Process.* **3**, 18 (1959).
(15) Natl. Acad. Sci. - Natl. Research Council, "Data on Chemicals for Ceramic Use," Bull. No. **118**, Washington, D.C. (1949).
(16) Ricci, J.E., "Guide to the Phase Diagrams of the Fluoride Systems," **ORNL-2396**, Nov. 19, 1958.
(17) Spangenberg, K., *Z. Krist.* **57**, 494 (1923).
(18) Swanson, H.E., Tatge, E., *Joint Committee Fellow Reports, Natl. Bur. Std.*, 1949.
(19) Thoma, R.E., Ed., "Phase Diagrams of Nuclear Reactor Materials," **ORNL-2548**, pp. 52–3, 60–1, Nov. 6, 1959.
(20) White, G.D., Oak Ridge National Laboratory, Oak Ridge, Tenn. unpublished data, 1955.
(21) Zachariasen, W.H., *Acta Cryst.* **7**, 792 (1954).

RECEIVED for review November 24, 1964. Accepted April 18, 1965. Research sponsored by U.S. Atomic Energy Commission under contract with the Union Carbide Corporation.